Molecular BioSystems

Accepted Manuscript

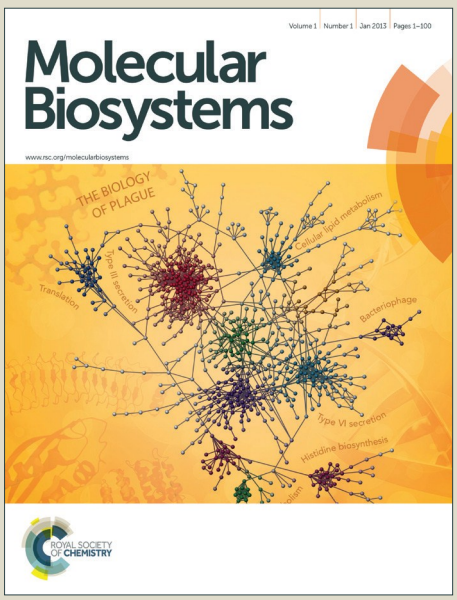

ROYAL SOCIETY OF CHEMISTRY

www.rsc.org/molecularbiosystems

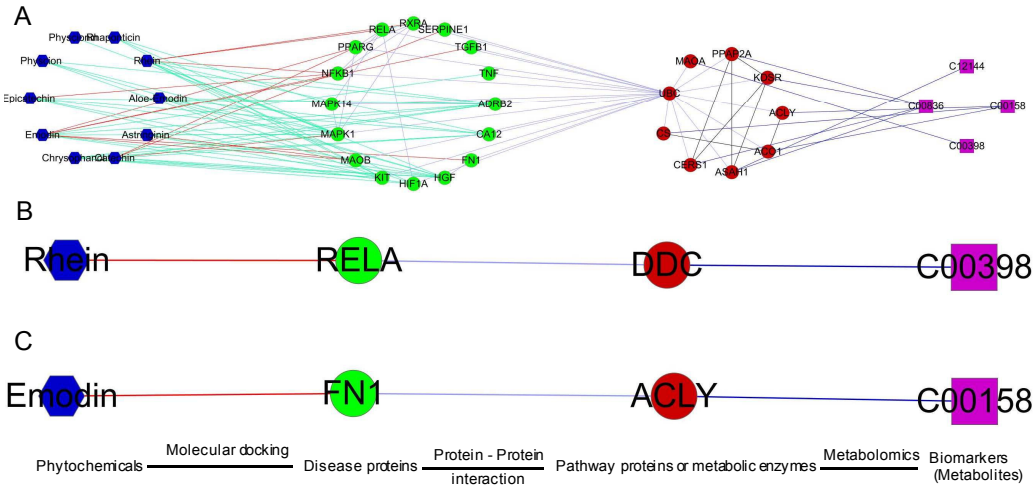

The study on material basis and mechanism for anti-renal interstitial fibrosis efficacy of rhubarb through integration of metabonomics and network pharmacology

Zheng Xiang*, Hao Sun, Xiaojun Cai, Hui Chen, Xiaoyong Zheng

School of Pharmaceutical Sciences, Wenzhou Medical University, Wenzhou 325035, China

Corresponding Author

Zheng Xiang

*Tel/Fax: +86-577-86689949. E-mail: XZH0077@126.com.

ABSTRACT: The cooperative material basis of multi-component and multi-target mechanism of action of Traditional Chinese Medicine (TCM), is difficult to elucidate because of the current lack of appropriate techniques and strategies. In this paper, we focus on rhubarb treatment of renal fibrosis. Molecular docking, metabolic pathway enrichment, and network pharmacology methods were used to theoretically determine the interaction between the components of the rhubarb and disease targets related to renal fibrosis. Moreover, the methods of metabolomics, serum pharmacochemistry, histopathology and immunohistochemistry were used for the model group, sham-operated group and rhubarb administration group, to reveal the active components and mechanisms of rhubarb. Finally, the experimental and theoretical results were integrated and comprehensively analyzed. Results indicated that anthraquinones and flavanols, such as rhein, emodin, catechin, and epicatechin, were the main active components of rhubarb. These active conponents play synergistic therapeutic efficacies through regulating the abnormal accumulation of extracellular matrix, controlling the release of inflammatory factors, and maintaining the balance of coagulation and fibrinolysis. Our study showed that the integration of metabolomics and network pharmacology is a powerful strategy for discovering active components of TCMs and for elucidating their mechanisms.

Keywords: Metabonomics; network pharmacology; serum pharmacochemistry; rhubarb; renal interstitial fibrosis

Introduction

Chronic kidney disease (CKD) has become one of the major threats to the world's public health [1]. Renal interstitial fibrosis (RIF) is a common pathological consequence of all CKDs in end-stage renal diseases. Recently, in the United States, Europe, Japan, Australia, and China, a large-scale epidemiological survey on CKD indicated that the adult prevalence rate was up to 10 %, and approximately 0.2 % of CKD patients develop RIF [2, 3]. Current research indicates that RIF is a result of excessive deposition of the extracellular matrix (ECM) and proliferation of interstitial fibroblast caused by infection and immune factors [4], which include the alteration of multiple signaling pathways and biological processes [5, 6]. Therefore, RIF is a typical complex disease with multiple targets and requires the combinatorial intervention of multiple drugs. Rhubarb, a famous traditional Chinese medicine (TCM) has been widely used to clinically treat CKD [7]. Currently, more than 1000 studies have been published on the use of rhubarb for renal disease treatment [8-10]. However, for decades, because of the multiple components of rhubarb and complex mechanism of action, considerable efforts have been devoted to studying the components and mechanism of rhubarb, yet it remains a major unresolved problem.

Within the last 10 years, chemoinformatics, network pharmacology and systems pharmacology methods have been successfully applied in the discovery of the active component of TCMs and their mechanisms of action. Li established an algorithm termed NIMS (Network targetbased Identification of Multicomponent Synergy) [11] and the platform of TCM network pharmacology [12] in order to screen out synergistic drug combinations [13, 14]. A TCM systems

pharmacology platform was constructed by Wang et al [15], and this platform was used to successfully screen and determinate the multi-component and multi-target mechanism of action of TCMs [16]. In 2002, Wang et al, proposed TCM serum pharmacochemistry [17]. Presumably, the active components of TCMs will be useful in the curative therapy only if they reach a certain blood concentration and have appropriate bioavailability in the systemic circulation. After the study on Yin Chen Hao Decoction for decades, Wang *et al* basically determined its active components basis by serum pharmacochemistry method [18, 19] and then furthered the understanding of mechanism of action for protective effects on liver and gallbladder [20]. These virtual screening or experimental strategies and methods greatly narrowed down the selection of TCM's active components and their mechanisms.

In this work, we focused on using rhubarb to treat RIF. A strategy that integrates metabolomics, serum pharmacochemistry, network pharmacology, pathological tissue and immunohistochemical method was developed and applied to determine the main active components of rhubarb and to elucidate its multi-component, multi-target mechanism of action from a gene-protein-metabolite systems perspective. This study provides a theoretical basis for the treatment of RIF using rhubarb and enhances the methodological exploration of the discovery of TCM's active components.

Materials and methods

Our protocol involved six main steps, as follows: 1) molecular docking between phytochemical components in rhubarb and known target proteins and constructing a phytochemical component - target protein interaction network; 2) identifying active components that are absorbed into blood and constructing an absorbed component - target protein interaction network; 3) screening out biomarkers based on metabolomics and performing pathway enrichment analysis ($P < 0.05$); 4) constructing of an extended metabolite - pathway protein interaction network; 5) establishing component – protein – metabolite and subsequently finding the shortest path from the components to metabolites by bioinformatics methods; and 6) performing a mutual validation of histopathology, immunohistochemistry and literature search. The entire frame is shown in Figure 1.

Reagents and Materials

HPLC-grade methanol and acetonitrile were purchased from Merck (Darmstadt, Germany). The assay kits for serum creatine (Scr) and blood urea nitrogen (BUN) were purchased from Nanjing Jiancheng Bioengineering Institute (Nanjing, China). Formic acid and leucine enkephalin were obtained from Sigma-Aldrich (St. Louis, MO, USA). Rhein, physcion, aloe-emodin, emodin, catechin, epicatechin, chrysophanol, physcionin, rhaponticin and astringin with 98.0 % purity were purchased from Chengdu MUST Bio-Technology Co. Ltd (Sichuan, China). Ultrapure water (18.2MΩ) was prepared with a Milli-Q water purification system (Millipore, USA). All other chemicals used were of analytical grade.

Rhubarb (RH) was purchased from Wenzhou Tong Ren Tang Group Co., Ltd (Wenzhou, China). Dried and pulverized materials of RH (500 g) were ground and then refluxed with 4000 mL of water for 60 min, twice respectively. After cooling, the collection of extracted solution was filtered through 8 layers of gauze and was then condensed under decompression (Buchi, switzerland) to 250 mL (0.5 mL/g).

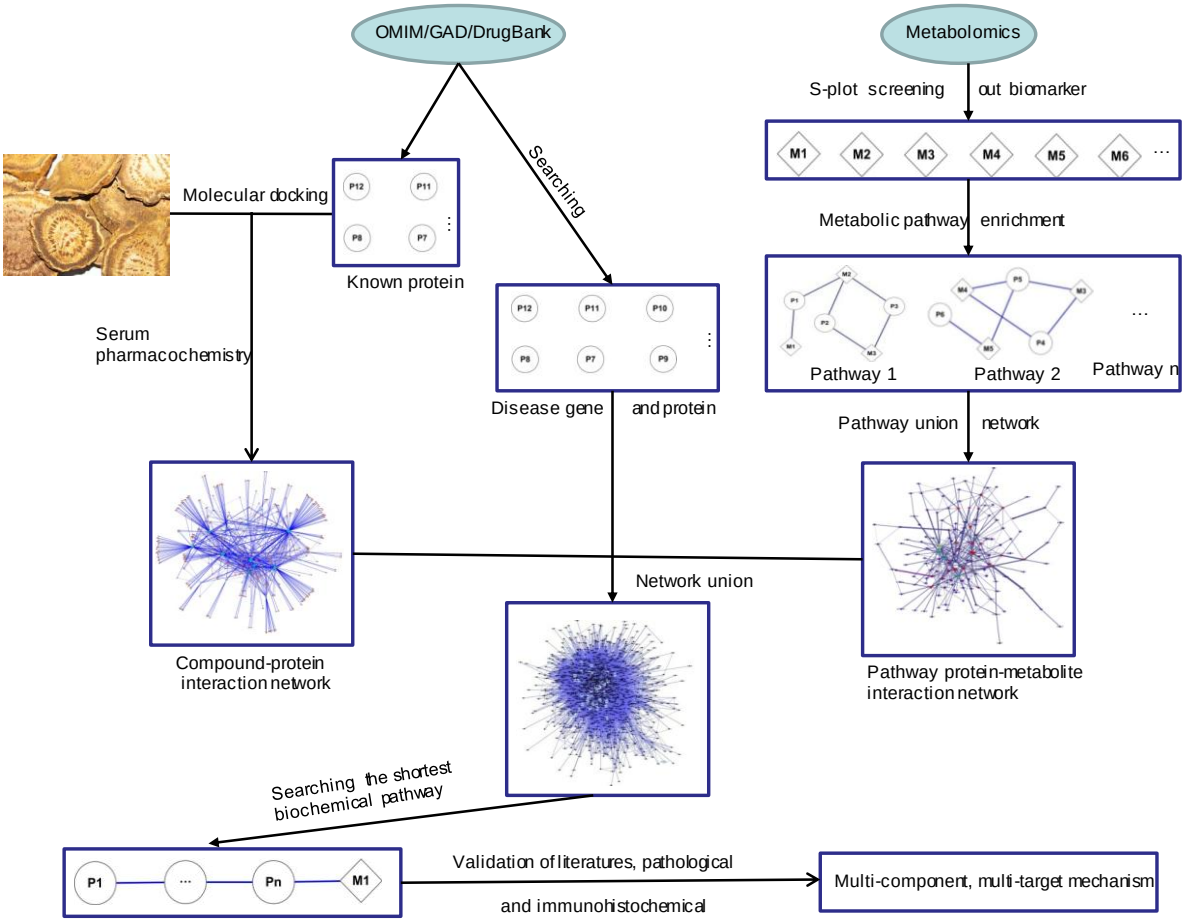

Figure 1. The entire framework of this work.

Animal Handling and Surgery

Twenty four male Sprague-Dawley rats (150 ± 10 g) were purchased from Laboratory Animal Center of Wenzhou Medical University (Wenzhou, China) and were kept in a specific pathogen-free (SPF) colony. They were fed with a certified standard diet and tap water ad libitum. All animals were kept in an animal room with a temperature of 22 ± 2 °C, a humidity of 50 ± 5 %, and a 12 h dark/light cycle. After 2 weeks acclimatization, the rats were randomly divided into three groups as follows: RH group (RHG) at a single dose of 0.5 mL/g, sham-operated group (SOG) and unilateral ureteral obstruction group (UUO). All experiments were performed in accordance with the approved animal protocols and guidelines established by Medicine Ethics Review Committee for animal experiments of Wenzhou Medical University.

The procedures on the UUO and RHG rats were carried out according to the operating procedure described previously [21]. In brief, under the anesthesia (10 % chloral hydrate, 3 mL/kg), the left ureter was isolated and completely ligated with 4–0 silk suture. The SOG underwent an identical surgical intervention except for ureter ligation. RHG was administered at a 8 mL/kg dose for continuous 21 days since the surgery, and the volume of normal saline was administered to SOG and UUO.

Sample Collection and Handling

On the 21st day after surgery, UUO, SOG, and RHG rats were anesthetized with 10 % chloral hydrate (3 mL/kg) by intraperitoneal injection, and the orbital blood was collected to determine the Scr and BUN. The serum was used for biochemical assay using a commercail kit and the

manufacturer's instructions were followed. The urine samples of UUO and SOG were collected on the 21st day, whereas RHG urine samples were collected on the 7th, 14th, and the 21st days. All samples were then centrifuged at 12000 *g* for 10 min. Subsequently, 100 μL of the supernatant was diluted to 200 μL with 100 μL of water. Finally, 5 μL of solution was injected for UPLC analysis.

A single dose of 0.5 mL/g was administered to six normal rats and 0.5 mL of blood was obtained from rats after 0.75 h. After 3000 *g* centrifugation, 100 μL of the plasma was extracted by 500 μL of ethyl acetate. The plasma extraction was dried by nitrogen gas and then dissolved in 100 μL of methanol : water (50 : 50). After 12000 g centrifugation, the supernatant was used to detect the serum pharmacochemistry of RH by UPLC-Q-TOF.

Histopathology and Immunohistochemistry

Fresh kidney tissues were excised from rats, stored in paraformaldehyde (4 %) for 24 h, and embedded in paraffin wax. Four-micrometer histological sections of the paraffin-embedded tissues were stained with hematoxylin-eosin (HE) and Masson. The ultrastructural change of kidney tissues was evaluated by using a transmission electron microscope. For Masson staining, under the 200 times microscope, 5 to 10 non overlapping fields of view under 200 × magnification were randomly selected for each specimen. Blue-green collagen deposition was considered a positive signal. The percentage rate of positive area versus total visible area in each slice was calculated, and its average value was regarded as the relative interstitial volume. The

semi-quantitative analysis criteria of Masson staining were set as follows [22]: 0 points, the percentage rate of positive area (< 2 %); 1 point, the percentage rate of positive area (2 % to 10 %) for mild lesions; 2 points, the percentage rate of positive area (11 % to 20 %) for moderate lesions; 3 points, the percentage rate of the positive area (21 % to 30 %) for severe lesions; and 4 points, the percentage rate of positive area (> 30 %) for very severe lesions.

Immunohistochemical determination of α-SMA, CTGF, and Col-I was established as follows: under 200 × magnification, 5 to 10 non-overlapping fields were randomly selected from tissue sections. The percentage rate of the positive area versus total visible area in tissue sections was calculated using Image Pro Plus software, and its average value was regarded as the relative interstitial volume.

Chromatography and Mass Spectrometry Conditions

Chromatographic analysis was performed in a Waters ACQUITY UPLC system controlled with Masslynx (V4.1, USA). An aliquot of 5 μL of sample solution was injected onto a BEH Shield C18 column (100 × 2.1 mm, 1.7 μm). Column temperature was set at 40 °C and the flow rate was 0.3 mL/min. The optimal mobile phase consisted of a linear gradient system of (A) 0.1 % formic acid in water and (B) 0.1% formic acid in acetonitrile: 0-1.5 min, B (1-10 %); 1.5-6.0 min, B (10-25 %); 6.0-10.0 min, B (25-50 %); 10.0-12.0 min, B (50-100 %); 12.0 -13.0 min, B (100 %); 13.0-14.0 min, B (100-1 %) and 14.0-15.0 min, B (1 %).

Mass spectrometry detection was performed using a Waters Micromass Q-TOF micro Synapt High Definition Mass Spectrometer (Waters, Milford, USA) equipped with electrospray ionization. The optimal conditions of analysis were as follows: source temperature was set at 120 °C, desolvation gas temperature was 350 °C, cone gas flow was 50 L/h, desolvation gas flow was 650 L/h, capillary voltage was 3.0 KV, sampling cone voltage was 50.0 V, extraction cone voltage was 4.0 V. A lock mass calibration of leucine-enkephalin (0.2 ng/mL) in water/acetonitrile (50:50, v/v) was continuously introduced in the mass spectrometer via the second ESI probe (Lock-Spray) at a flow rate of 100 μL/min, generating a reference ion for negative ion mode (*m/z* 554.2611) to ensure accuracy during the MS analysis. Data was acquired from *m/z* 50 to 1000 Da with a 0.3 s scan time and a 0.1 s interscan delay and processed further in MassLynx 4.1.

Pattern Recognition Analysis and Data Processing

The mass spectral data acquired was imported to Markerlynx (Masslynx software, version 4.1) for peak detection and alignment. The retention time and *m/z* data for each peak was determined by the software. Full scan mode was employed in the mass range of 50-1000 amu. The initial and final retention time was set at 0 and 12 min for data collection. All data was normalized to the summed total ion intensity per chromatogram, and the resultant data matrices were introduced to SIMCA-P+12.0 software for principal component analysis (PCA) and orthogonal partial least-squares discriminant analysis (OPLS-DA). Prior to PCA, all variables obtained from data matrix

were mean-centered and scaled to Pareto variance. PCA, an unsupervised pattern recognition approach, is used to reduce the dimension of UPLC-MS data and to disclose intrinsic clustering of samples. To maximize the differences in inter-class discrimination and minimize the differences in intra-class discrimination, the data were further analyzed using OPLS-DA method. Variables with higher VIP value were considered as potential biomarkers and subjected to further MS/MS identification of the molecular formula with the help of available biochemical databases, such as HMDB (http://www.hmdb.ca/), METLIN (http://metlin.scripps.edu/) and MassBank (http://www.massbank.jp/). Other statistical analyses including one-way analysis of variance (ANOVA) and independent sample t-Test were performed with R programming language. A p-value (< 0.05) was considered statistically significant.

Pathway enrichment analysis of biomarkers and enrichment network construction

A comprehensive tool suite for metabolomics data analysis MetaboAnalyst 2.0, was used to enrich the pathway of biomarkers. The proteins from the enrichment pathways ($P < 0.05$) were extended to their nearest neighbors, and subsequently, a new metabolite - pathway protein interaction network (MPPI) was constructed by BioGenet [23].

Finding phytochemical components, screening out candidate gene and molecular docking

The phytochemical components of RH were collected from Comprehensive Natural Products in TCM [24] and Reaxys data (https://www.reaxys.com). These phytochemical components were

filtered by Lipinski's 'rule of five' [25]. Ligands of molecule-protein complexes related to CKD targets were used as positive drugs and were collected from Drugbank[26, 27]. The optimization of all molecular structures was based on MMFF94 force field, and the stop condition was set to the RMS of potential energy (< 0.001 Kcal $Å^{-1}$ mol^{-1}).

Genes associated with CKD were collected by searching the Online Mendelian Inheritance in Man (OMIM) [28] database with keyword 'renal or kidney', Genetic Association Database (GAD) [29] with keyword 'chronic kidney disease'. In the OMIM database, the searched genes unrelated to CKD, such as renal carcinoma gene, were manually deleted. In the GAD database, the association with CKD was shown as "Y". 36 known targets related to CKD (Table S1) were collected from Therapeutic Target database [30] and DrugBank [31]. Their X-ray crystal structures were downloaded from PDB. Molecular docking between phytochemical components (or positive drugs) and CKD's target proteins was conducted using the free available software AutoDock Vina [32]. The docking scores between known drugs or ligands of molecular-protein complex, and known target proteins were used as the cutoff value to screen out potential active components from RH. For all components and target proteins, effective docking was defined by the following conditions: the docking score between a component and a target was less than the corresponding cutoff value of the positive drug and also less than −5.0 kcal/mol [33]. A component and a protein can be linked with an edge. As a result, a phytochemical component – target protein interaction network (PTPI) can be constructed and displayed by Cytoscape 2.8.

Construction and analysis of component – protein – metabolite interaction network

According to the collected candidate genes and proteins related to CKD, a protein - protein interaction network (PPI) was built by Cytoscape 2.8. Subsequently, PPI combined with PTPI was used to establish a new phytochemical component - target protein interaction network (NPTPI). The nodes of NPTPI were filtered according to the result of RH serum pharmacochemistry and then got an absorbed phytochemical component - protein interaction network (APPI). APPI combined with MPPI was then used to establish a component – protein - metabolite interaction network (CPMI). At last, the shortest biochemical pathway was obtained through searching the shortest network distance from CPMI.

Table 1. The content of serum creatinine and urea nitrogen in rats and the results of collagen semi-quantitative in Masson staining ($\bar{x} \pm s$, n=8)

Groups	Scr (μmol/L)	BUN (mmol/L)	Relative volume of renal interstitial (%)
SOG	109.07 ± 9.23^{b}	6.47 ± 0.61^{b}	0.83 ± 0.48^{b}
UUO	$152.67 \pm 4.62^{a,b}$	$8.73 \pm 0.18^{a,b}$	$31.32 \pm 2.50^{a,b}$
RHG	$120. 3 \pm 3.60^{b}$	6.33 ± 0.70^{b}	$10.83 \pm 1.72^{a,b}$

[a]: $P < 0.05$ (SOG, control group); b: $P < 0.05$ (UUO, control group).

Results and Discussion

Biochemical test of Scr and BUN

The Scr and BUN levels are shown in Table 1. Scr and BUN in UUO significantly increased on the 21st day, thereby suggesting that kidney tissue was obviously damaged. No statistical difference was found in the levels of Scr and BUN between RHG and SOG, thereby suggesting that rhubarb could significantly reduce the Scr and BUN, in agreement with results from literature [8, 34, 35].

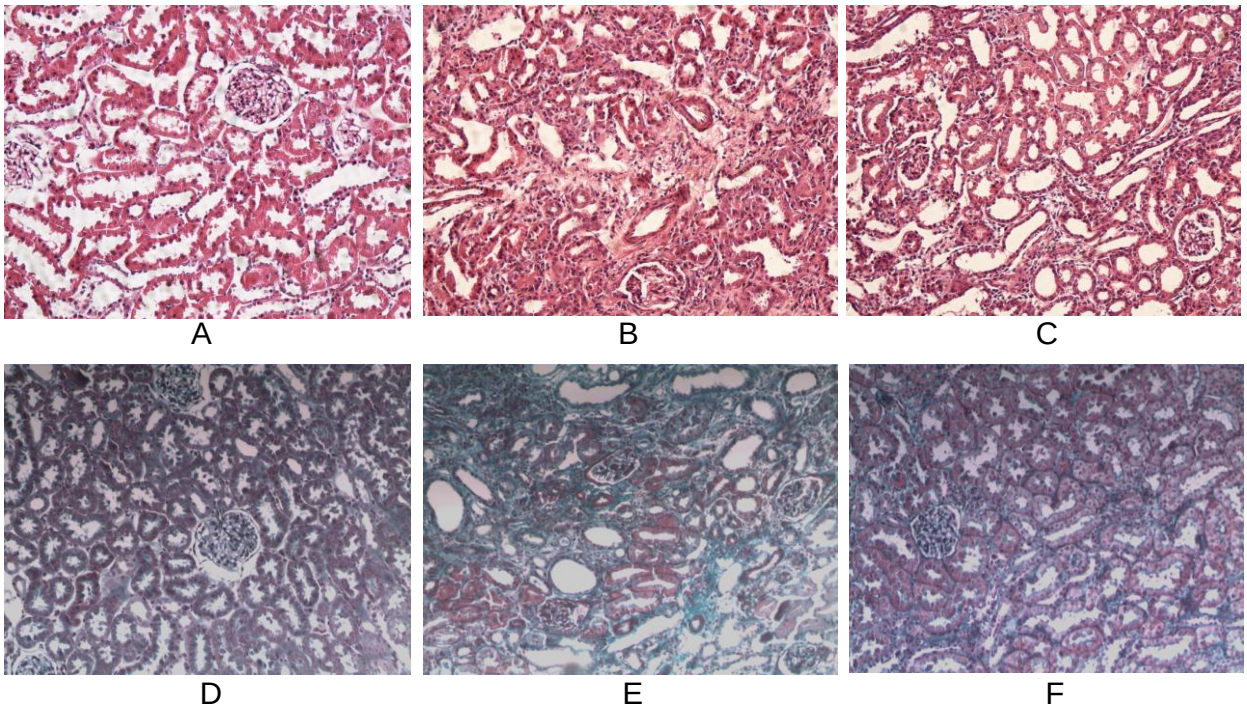

Figure 2. Representative light photomicrographs of kidney tissue sections stained with HE (SOG (A), UUO (B) and RHG (C)) and Masson (SOG (D), UUO (E) and RHG (F)).

HE and Masson staining

The results of HE staining are shown in Figure 2A to Figure 2C. The glomerular and tubular structures in SOG were normal (Figure 2A). However, renal parenchyma significantly became thinner (Figure 2B). Stromal diffuse infiltration of inflammatory cells, collagen formation, and

evident fibrosis formation in UUO were observed. RHG showed minimal inflammatory cell infiltration of renal interstitial tissue and hyperplasia of fibrous tissue compared with UUO. Tubular dilatation and atrophy of RIF was also significantly improved.

Masson staining is shown in Figure 2D to Figure 2F. The collagen staining in SOG was mainly located in the tubular basement membrane (Figure 2D). However, renal interstitium markedly widened and collagen fibers significantly increased in UUO (Figure 2E). The collagen deposition on renal interstitium in RHG (Figure 2F) was significantly reduced, indicating the a good therapeutic effect of rhubarb. Results of collagen semi-quantitative analysis by Masson staining are shown in Table 1. The relative volume of renal interstitial tissue in RHG was higher in SOG, and significantly lower in UUO. The histopathological result of HE and Masson staining showed that rhubarb could significantly delay the progression of RIF.

Table 2. The expression rate of positive area of α-SMA, CTGF, Col I in renal tissue.

Group	α-SMA	CTGF	Col-I
SOG	0.8 ± 0.34^{b}	3.41 ± 1.89^{b}	3.87 ± 1.47^{b}
UUO	$6.32 \pm 2.05^{a,b}$	$15.62 \pm 6.63^{a,b}$	$16.26 \pm 2.97^{a,b}$
RHG	$2.58 \pm 0.93^{a,b}$	$5.35 \pm 1.56^{a,b}$	$5.36 \pm 2.47^{a,b}$

[a]: $P < 0.05$ (SOG, control group); b: $P < 0.05$ (UUO, control group).

Immunohistochemistry

The semi-quantitative analysis results of α -SMA, CTGF, and Col-I in three groups are shown in Table 2. The average positive area expression rate of α -SMA, CTGF and Col-I in UUO was significantly higher than that in SOG. RHG's positive average area expression rate was higher than in SOG, but significantly lower than in UUO. Statistically significant differences were found in the positive average area expression rate of α -SMA, CTGF, and Col-I in the three groups, suggesting that rhubarb greatly alleviated the pathological degree of RIF.

Construction of a phytochemical component - protein network

According to Lipinski's rule of five [43], a total of 113 phytochemical components (Table S2) were selected from rhubarb and they were then optimized with MM79 force field. The 3D structures of 36 known target proteins were obtained from the PDB database. The natural ligands binding with target proteins were regarded as positive drug. After the pretreatment on target proteins, the positive drug and 113 phytochemical components were docked with 36 known target proteins by Autodocking Vina. Table S3 shows the docking scores of positive drugs. If the docking scores of a phytochemical component and a target protein was lower than that of a positive drug, they was linked by an edge. Such as, a phytochemical component - target protein network (PTPI) was constructed by Cytoscape 2.8 (Figure S1.A). This network consisted of 85 component nodes and 36 protein nodes. The topological property of PTPI was characterized with a power-law rule ($Y = 107.27X^{-0.917}$, $R = 0.936$). The average node degree of each phytochemical is 2.86, while the average node degree of each target is 22. The node degrees of rhein, chrysophanol and monorhein-anthranol were greater than 6 and the node degrees of MAPK1,

KIT, HGF and MAPK14 were greater than 30. These results showed that one compound can act on multiple proteins, and a protein can also be affected by multiple compounds [36, 37].

The collection of disease genes and target proteins from OMIM, GAD, Drugbank and TTD database were listed in Table S1. In order to study the disturbance of disease protein caused by up - or down - regulation of target proteins, these collected genes and proteins were mapped into BIOGRID, INTACT, MINT, DIP, BIND and HPRD database in order to construct disease protein - protein network (PPI) by BioGenet (Figure S1.B). This network consisted of 130 nodes and 78 edges with 43 (33.3 %) nodes linked to 64 (82.1 %) edges forming the largest cluster, suggesting that many disease proteins tend to interact with each other [38]. A new phytochemical component - protein interaction network (PPIN) was established by computing the union of both PTPI and PPI (Figure S1.C). This network represents the interactions of phytochemical components and known target proteins, and the relationship between the target proteins and disease proteins, suggesting that the disturbance of target protein would result in the up - or down - regulation of adjacent disease protein.

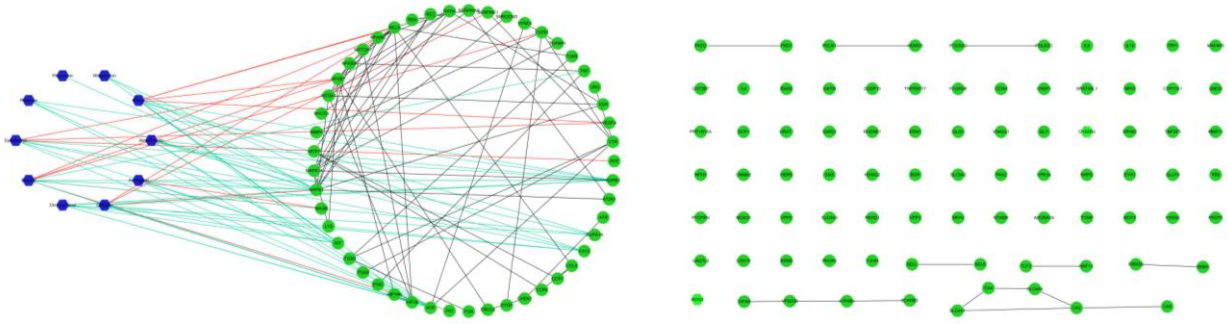

Figure 3. The absorpted phytochemical component - target protein network. Phytochemical components and proteins are labeled as the blue hexagon and green circles, respectively. The interactions between phytochemical components and proteins, and between known target proteins and disease proteins are linked by the cyan and black edges, respectively. If the interactions between phytochemical components and proteins is validated by the literature, this interaction was linked by red edge.

Construction of an absorbed phytochemical component – protein network

Plasma samples were prepared according to 2.3 section. The typical UPLC-Q-TOF chromatogram of samples was shown in Figure S2. In the identification process of the phytochemical components absorbed into blood, we focused on 85 phytochemical components in PPIN. At last, according to the mass spectra and retention time of reference compounds, ten components absorbed into blood were identified and labeled as Figure S2, which was consistent with literatures [39-45]. As a result of the low content or bioavailability of phytochemicals, 75 out of 85 phytochemicals were not detected. After removing 75 nodes (phytochemical) in PPIN, a new absorbed phytochemical component - protein interaction network (APTP) was established (Figure 3). This new network included 142 nodes, connected by 141 edges, which can characterize the interaction between 10 absorbed phytochemical components and known target proteins. The interactions between emodin and the protein of TGFB1, NFKB1 and PPARG, between rhein and the protein of NFKB1, RELA, RXRA and VEGFA, between epicatechin and

the protein of ACE, NFKB1 and VEGFA, and between catechin and the protein of SERPINE1, MAPK1 and PPARG were experimentally validated and were collected in STITCH [46], HIT [47], TCMID [48] and TcmSP [49] database, suggesting that the molecular docking method can be used to predict the interaction between molecules and targets.

Metabonomic study of urine

To optimize the experimental conditions, metabolic profiles of a small batch of QC urinary samples were acquired in positive and negative mode, respectively. We observed that higher noise and matrix effect in ESI positive mode led to a higher baseline, which resulted in the neglect of some metabolites with low abundance and the concomitance of multiple adductions. Therefore, considering maximization of the number of detectable metabolites and the quality of data acquired, full-scan detection was eventually set as ESI negative mode. After careful optimization of the gradient elution for the chromatography and capillary voltage, flow, and temperature of desolvation gas for the mass spectrometry detector, the optimal parameters were listed in Section 2.5. The representative urine chromatogram of UPLC-Q-TOF in negative ion mode was shown in Figure S3. After processing as Section 2.6, a list of more than 4000 compounds could be exported for each sample. The precision and repeatability of the UPLC-Q-TOF method was validated by the duplicate analysis of six injections of the same QC samples and six parallel samples prepared using the same preparation protocol, respectively. The relative standard deviations of the peak retention time and area value was less than 5.0 %. The resulting

data showed that the precision and repeatability of the proposed method was satisfactory for metabonomic analysis.

The sample data is imported into SIMICA by Markerlynx 4.1. PCA is used for pattern recognition of UUO, RHG and SOG. PCA score plot is shown in Figure 4A. In essence, each symbol in Figure 4A represent the 2-dimensionality projection of each sample. In order to narrow the pattern space of the similar types of samples and expand the pattern space of different types of samples, a supervised pattern recognition method, OPLS-DA is applied to distinguish all samples. The results are shown in Figure 4B, indicating that the better distinction of different groups are obtained. The trajectory changes of urine metabolic profilings of RHG on the 7^{th}, 14^{th} and 21^{st} days displayed that the metabolic profiling on 21^{st} day was close to SOG, suggesting that rhubarb has obvious effect on relieving the severity of RIF. R^2Y provides an estimate of how well the model fits the Y data, while Q^2Y is an estimate of how well the model predicts the Y. Both Q^2Y (0.73) and R^2Y (0.968) indicated an excellent predictive ability.

Variables (metabolites) that significantly contributed to the clustering and discrimination are selected according to a threshold of variable importance in the projection values (VIP > 2), which could be generated after OPLS-DA processing. In order to select potential biomarkers, these differential metabolites are also validated using Student's t-Test. The critical p-value is set to 0.05 for significantly differential variables in this work. Based on the criterion above, 30 significantly different endogenous metabolites were screened out for further study. Their MS and MS/MS information was obtained by searching freely accessible databases of KEGG, Metlin, MassBank and HMDB utilizing detected molecular weights and elemental compositions. As a

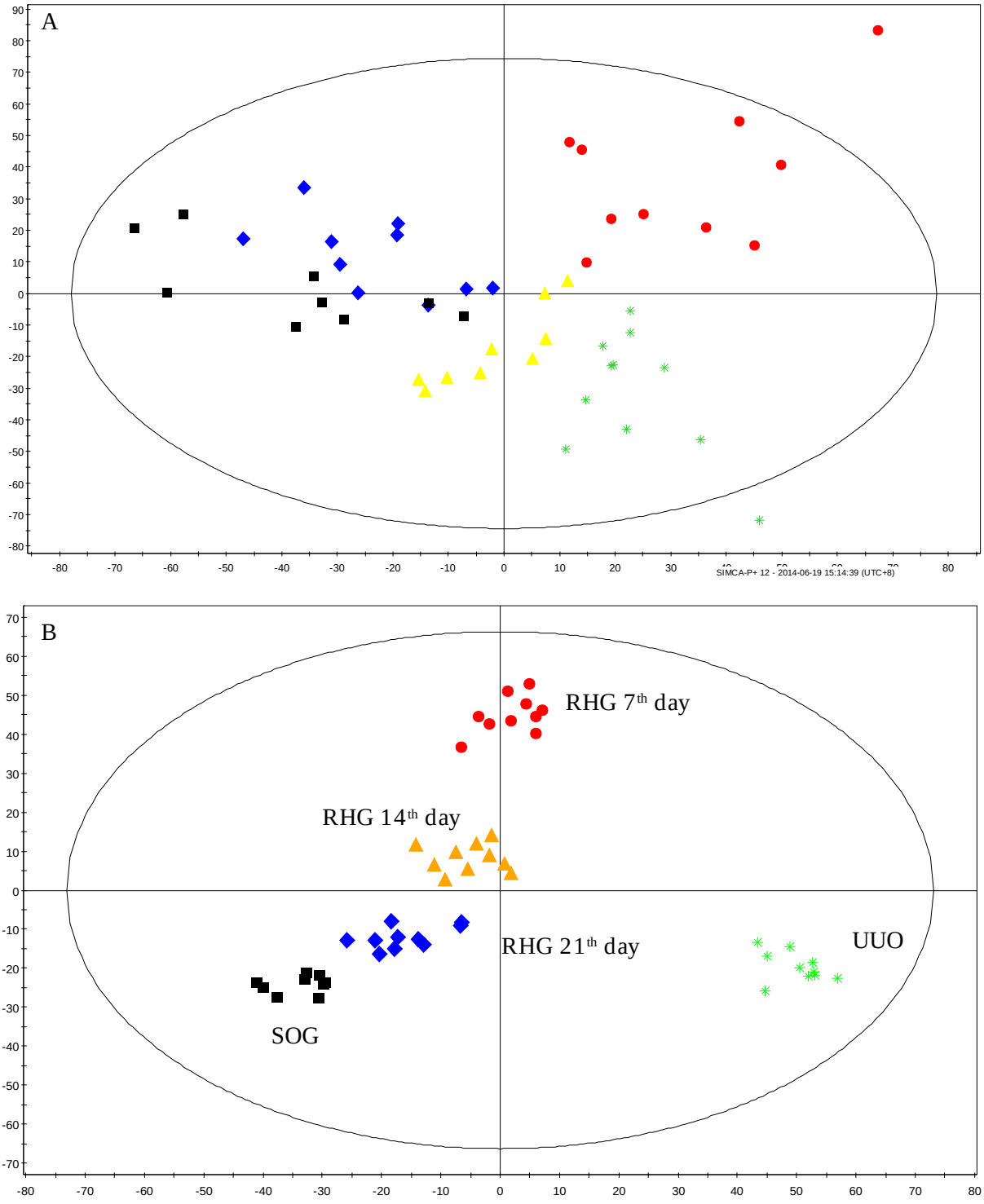

Figure 4. PCA (A) and OPLS-DA (B) scores plots of rat urine data on days RHG (7^{th}, 14^{th}, and 21^{st} day), SOG (21^{st}) and UUO (21^{st}).

result, 22 metabolites are identified on the basis of accurate elemental compositions and context of retention time with available databases, as is listed in Table S4. MetaboAnalyst 2.0 software is used to enrich the signal pathway of 22 biomarkers and then select significant enrichment pathway from KEGG database according to hypergeometric distribution ($P < 0.05$). The enrichment pathways included tryptophan metabolism, ascorbate and aldarate metabolism, citrate cycle, riboflavin metabolism and sphingolipid metabolism. The four signaling pathways are merged to build a metabolite - protein network (MPI), which included 374 nodes (74 proteins), 490 edges and 180 isolated nodes (Figure S4.A).

Typically, the transfer of biological information from gene to the metabolite requires a multi-step biochemical cascade [50, 51]. To obtain the signal transfer process of RIF, 74 proteins extracted from four signal pathways expanded their most neighboring nodes by BioGenet to build an extended pathway protein - protein network (EPPI) (Figure S4.B). This network consisted of 721 nodes and 8613 edges, thereby providing an important bridge for the biological information transfer process from the disease gene, and protein to the metabolite. A large cluster of 709 (98.3 %) nodes was formed, thereby suggesting that these nodes could connect with each other through one or more network distances. MPI and EPPI were merged into a new metabolite - protein interaction network (NMPI) (Figure S4.C). This network included the 1023 nodes. Out of the 1023 nodes, 838 (82.0 %) formed the largest cluster linked by 9099 edges, thereby reflecting the interaction and relationship between biomarkers and proteins. The up- or down- regulation of proteins or metabolic enzymes resulted in changes in the concentration of biomarkers.

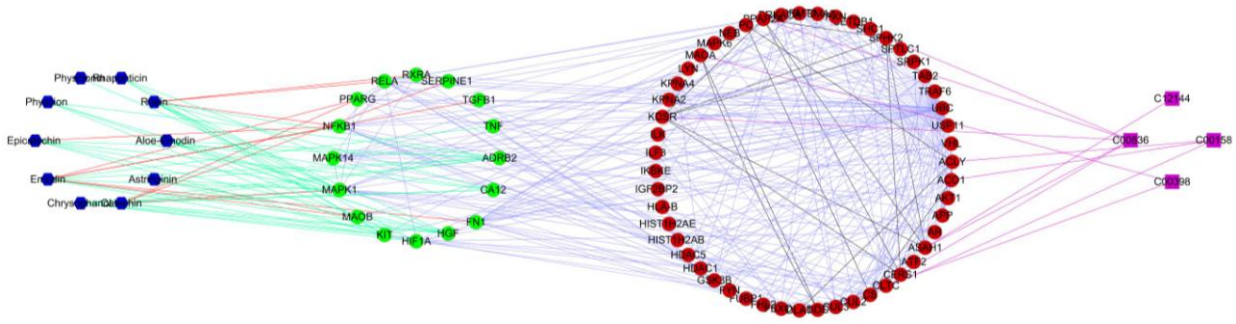

Figure 5. Component – protein - metabolite network. The active components, disease proteins, pathway proteins and metabolites are represented by the blue hexagon, green circles, red circles and purple squares, respectively. The interactions between phytochemical components and proteins and between proteins and proteins are linked by the cyan and blue edges, respectively. The interactions between metabolites and proteins were validated by literature and linked by purple edges.

Construction and analysis of component – protein – metabolite network

To obtain the entire biological process from absorbed phytochemical components to metabolites (biomarkers), a component - protein - metabolite interaction network (PPMI) was established through the integration of APTP (Figure 3) and NMPI (Figure S4.C), as shown in Figure S5. This network consists of 1159 nodes, including one cluster of 945 nodes connected by 9873 edges. This network included absorbed phytochemical components, disease proteins, pathway proteins, and biomarkers. The absorbed phytochemical components acting on target proteins would cause the up- or down- regulation of metabolic enzymes, thereby resulting in the changes

in concentration of biomarkers. The newwork characterizes the process and pathway of the biological information transfer from gene – protein – metabolite viewpoints. The biological information transmission tended to follow the shortest path [52, 53]. We consider the absorbed phytochemical components as the initial node and the biomarkers (metabolites) as the terminal node. The shortest network path with less than 4 steps was identified from Figure S5, and the result is shown in Figure 5, which represents the entire biological process from components to biomarkers.

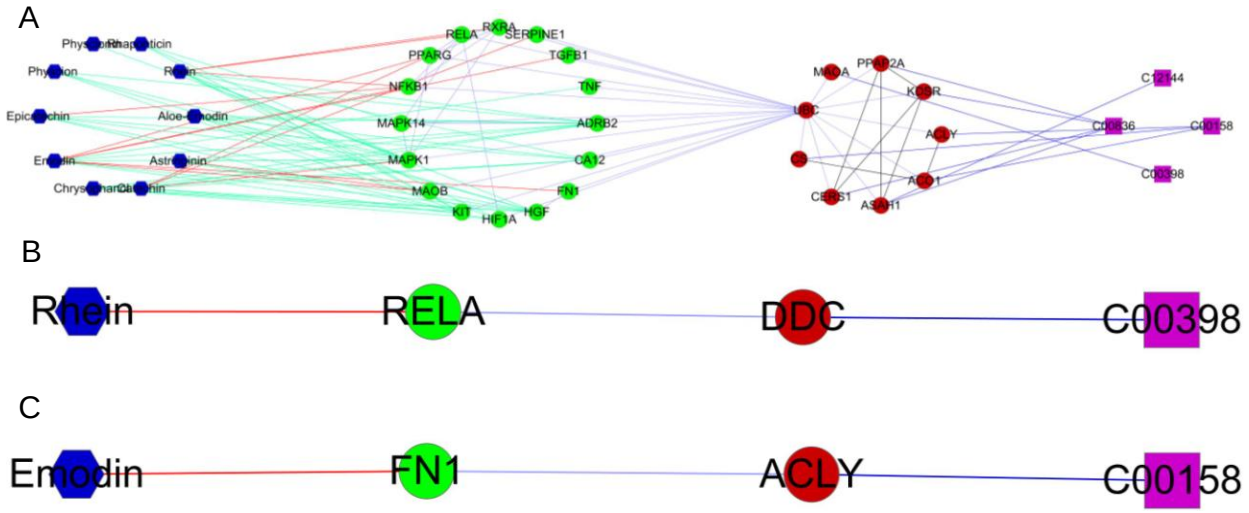

Figure 6. Sub-network of component – protein - metabolite network. Four paths from components to metabolites (A) and three paths from components to metabolites (B and C).

As shown in Figure 6, 10 absorbed phytochemical components (aloe-emodin, astringinin, catechin, chrysophanol, emodin, epicatechin, physcion, physcionin, rhaponticin and rhein) interacted with 16 target proteins, including ADRB2, CA12, FN1, HGF, HIF1A, KIT, MAOB, MAPK1, MAPK14, NFKB1, PPARG, RELA, RXRA, SERPINE1, TGFB1, and TNF. These

proteins can be related to four biomarkers through pathway proteins. Figure 6 show that the multiple connection pathways from disease proteins to four biomarkers. For the biological process with four pathways (Figure 6A), ubiquitin C (UBC) was used as the sole node connecting all known disease proteins based on the literature [55]. Figures 6B and 6C showed that the biological process only had three pathways from the absorbed phytochemical components to the biomarkers.

The abnormal accumulation of ECM is an important biochemical process of CKD [56]. Under normal circumstances, the accumulation and degradation of ECM is in equilibrium. Renal tubular cell injury caused by external stimulation resulted in the secretion of the TGF beta cell factor which could stimulate fibronectin (FN) secretion, and reduce the degradation of ECM, and thereby resulting in the abnormal accumulation of ECM. As shown in Figure 6A, emodin suppressed TGF-beta 1 and FN overexpression via inhibition of NF-kappa B activation [57, 58], thereby reducing the synthesis of ECM [59, 60]. Moreover, fibrosis would increase the secretion of UBC and accelerate the protein ubiquitin degradation of TGF-beta 1 and FN [61, 62], which contributes to the equilibrium of ECM. Hepatocyte growth factor (HGF) was secreted by mesenchymal cells and could stimulate matrix invasion. HGF has a central role in angiogenesis, tumorigenesis, and tissue regeneration. HGF and FN form a complex, which enhances endothelial cell migration through the activation of the PI-3 kinase pathway [63]. Emodin specifically inhibits the mitogenic effect of HGF [64]. A significant reduction in serum levels of HGF has been observed after the treatment with epicatechin [65]. Rhein can significantly elevate

the levels of HGF in the renal tissues and reduce the contents of fibronectin and collagen IV in the ECM [66]. Monoamine oxidase B (MAOB) in serum and the connective tissue can promote the maturation of the connective tissue and participate in the final stages of maturation bridge formation, and resulting in the binding of collagen and elastin proteins. Emodin and astringinin can significantly inhibit MAOB and reduce the formation of collagen [67, 68], which is consistent with the results of immunohistochemistry. These components act on important proteins involved in the biological process of accumulation and degradation of ECM, because they sustain the equilibrium of accumulation of ECM and delay the pathological progress of RIF. The imbalance between coagulation and fibrinolysis is an important pathophysiological change in the development of glomerular sclerosis [69]. Thrombin increases fibrin deposition in glomeruli through the up-regulation of the expression of plasminogen activator inhibitor (PAI), and inhibites the degradation of mesangial matrix thereby leading to the accumulation of ECM and glomerulosclerosis. Thus, balance is promoted between coagulation and fibrinolysis. SERPINE1 is a serine protease inhibitor that functions as the principal inhibitor of tissue plasminogen activator and urokinase [70]. The activation of plasminogen leads to fibrinolysis (degrades blood clots). Catechin and epicatechin can prevent TNF--mediated PAI production [71, 72], thereby reducing the expression of SERPINE1. The decrease in the expression of SERPINE1 can inhibit the expression of PAI, reduce fibrin deposition and maintain the balance between coagulation and fibrinolysis.

Under hypoxia, hyperglycemia and proinflammatory cytokines and other stimuli, kidney cells release chemokines, which result in inflammatory cell infiltration into tubulointerstitial tissue and produce fibrosis factor EGF-2 [73]. This case induces the involvement of small tube cells in the processes of myofibroblasts proliferation and secretion of extracellular matrix, thereby resulting in the extension of the lesion from the glomerular to tubulointerstitial regions and worsening the condition. Proteins, such as HIF1A, PPARG, NFKB, RELA and RXRA, were related to the process of hypoxia, inflammation, and infection [74, 75]. Therefore, the prevention of hypoxia and infection protects the kidney tissue from damage. Epicatechin, emodin and rhein can inhibit the activation of NF-kappa B, thereby reducing angiogenesis and inflammation [76-78]. Peroxisome proliferator-activated receptor gamma decreases the inflammatory response of many cardiovascular cells. Rhein inhibits the PPAR-gamma transactivity and the expression of its target genes [79]. Catechin promotes adipocyte differentiation and increases sensitivity to insulin partly via the direct activation of PPAR gamma [80]. These components prevent the release of proinflammatory cytokines and inhibit the occurrence of RIF in the priming phase [5].

RIF process is usually accompanied by the increase of UBC [69, 81, 82], which will accelerate the degradation of ubiquitinated protein, thereby down-regulating metabolic enzymes of PPAP2A [83], CERS1 [84], KDSR [85], CS [86], ASAH1 [62], ACLY [87], MAOA [88] and ACO1 [89]. Monoamine oxidase A is an isozyme of monoamine oxidase, which decreases the conversion rate of tryptamine to indole-3-acetaldehyde decrease, thereby leading to an increased concentration of tryptamine [90]. Citric acid is an important intermediate of the citric acid cycle, which is produced by the

catalytic reaction of aconitate hydratase (ACO1), citrate synthase (CS), and ATP citrate (pro-S) -lyase (ACLY) [91]. The ubiquitin degradation of CS, ACLY, and ACO1 decreases the production of citric acid. The degradation of acid ceramidase decreases catalytic rate of reaction of phytosphingosine, thereby reducing its content [92]. Sphinganine blocks postlysosomal cholesterol transport by inhibiting low-density lipoprotein-induced esterification of cholesterol. KDSR, ASAH1, and PPAP2A are the biochemical metabolism enzymes that produce sphinganine [93]. A decrease in KDSR, ASH1, and PPAP2A lowers sphinganine content. In summary, the decrease in concentration of metabolites, such as citric acid, phytosphingosine and sphinganine, or the increase of tryptamine is consistent with the results of metabonomics.

As shown in Figure 6B, rhein can inhibit the expression of RELA protein, thereby resulting in the decrease of aromatic L-amino acid decarboxylase (DDC) expression [94]. DDC is a lyase enzyme that catalyzes tryptophan to tryptamine, and its down-regulation will slow down the catalytic rate of tryptamine. Figure 6C indicates that emodin suppressed HG-induced cell proliferation and FN expression in rat mesangial cells by inhibiting the p38-MAPK pathway, which involves CREB, PPAP-γ, and CTGF [58]. The increase of FN1 results in the up-regulation of ATP citrate lyase [87]. ATP-citrate lyase is responsible for catalyzing the conversion of citrate and CoA into acetyl-CoA and oxaloacetate [95], and can accelerate the conversion rate of citric acid, thereby reducing its concentration. The concentration changes of citric acid and tryptamine are consistent with the metabolomics results. Figure 6B and 6C show two intact biological

process from components, and proteins to metabolites, thereby suggesting that network pharmacology and metabolomics approaches play an important role in systems pharmacology [96].

In summary, RIF involves multiple biological processes, such as the abnormal accumulation of ECM, the release of inflammatory factors and the balance of coagulation and fibrinolysis. These processes are mutually staggered. The multiple active components in rhubarb can target the multiple proteins in the disease biological network to regulate and restore the network equilibrium, thereby controlling the occurrence and development of RIF.

Conclusion

The metabonomics approach provides a tool for quantitatively describing the changes of endogenous metabolites of biological systems affected by external physical, chemical and environmental stimuli, which greatly contributed to understanding the mechanisms of action of TCM [97]. However, the disturbance of metabolites usually involves a multi-step biochemical cascade of reactions related to the disease genes and proteins. Thus it is difficult for metabonomics to explore TCM's multi-component mechanism from the "gene-protein-metabolite" molecular network viewpoint. The use of network methods to identify the association of disease genes and proteins with metabolites is rational because of the interactions between genes, proteins, and metabolites. In this paper, the integration strategy of network pharmacology and metabolomics was used to study the effective components and mechanism of action of rhubarb in RIF treatment. The result was also confirmed by conventional assessment,

which involved serum biochemistry, histopathological and immunohistochemical assays. Results indicated that the anthraquinone (rhein and emodin) and flavanols (catechin and epicatechin) were the main active substances and that play a therapeutic role in RIF by targeting the proteins related to inflammation, infection and fibrosis. Research shows that the integration strategy is a powerful tool for rapid screening of active multi-components from TCM and for revealing the mechanism of action of multi-targets. Results of this study are of great significance in innovative drug development from the gene - protein - metabolite overall viewpoint to explain the action process of multi-component drugs.

Competing interest

The authors declare that they have no competing interests.

Author Contributions

The manuscript was written through contributions of Zheng Xiang. All authors have given approval to the final version of the manuscript. Conceived and designed the experiments: Zheng Xiang. Performed the experiments: Xiaojun Cai, Hui Chen, Xiaoyong Zheng and Zheng Xiang. Analyzed the data: Zheng Xiang and Hao Sun.

ACKNOWLEDGMENT

The authors acknowledge financial support from the National Natural Science Foundation of China (No. 81001614) and the Nature Foundation Committee of Zhejiang Province, China (Y2100317 and LQ13H280001).

References

1. M. Rizzo, I. Iheanacho, F. E. van Nooten and D. Goldsmith, *Value Health*, 2013, **16**, A381-A382.
2. R. C. Atkins, *Kidney Int*, 2005, **67**, S14-S18.
3. R. T. Gansevoort, R. Correa-Rotter and B. R. Hemmelgarn, *Lancet*, 2013, **382**, 310-310.
4. J. S. Duffield, *J. Clin. Invest.*, 2014, **124**, 2299-2306.
5. Y. H. Liu, *Nat Rev Nephrol*, 2011, **7**, 684-696.
6. W. M. McClellan, *Med Clin N Am*, 2005, **89**, 419-+.
7. X. Wei, D. Hongzhu and M. Yun, *China Journal of Chinese Materia Medica*, 2002, **27**, 241-244.
8. H. Wang, H. X. Song, J. R. Yue, J. Li, Y. B. Hou and J. L. Deng, *Cochrane Db Syst Rev*, 2012.
9. X. M. Li and H. Y. Wang, *Adv Chronic Kidney D*, 2005, **12**, 276-281.
10. L. S. Li, *Nephrology*, 1996, **2**, S146-S150.
11. S. Li, B. Zhang and N. Zhang, *Bmc Syst Biol*, 2011, **5**, S10.
12. B. Zhang, X. Wang and S. Li, *Evidence-based complementary and alternative medicine : eCAM*, 2013, **2013**, 456747.
13. H. Li, L. Zhao, B. Zhang, Y. Jiang, X. Wang, Y. Guo, H. Liu, S. Li and X. Tong, *Evidence-based complementary and alternative medicine : eCAM*, 2014, **2014**, 495840.
14. X. Liang, H. Li and S. Li, *Mol Biosyst*, 2014.
15. C. Huang, C. Zheng, Y. Li, Y. Wang, A. Lu and L. Yang, *Briefings in bioinformatics*, 2013.
16. H. Liu, J. N. Wang, W. Zhou, Y. H. Wang and L. Yang, *J Ethnopharmacol*, 2013, **146**, 773-793.
17. W. Xijun, *World Science and Technology/Modernization of Traditional Chinese Mdicine*, 2002, **4**, 1-4.
18. X. J. Wang, W. J. Sun, H. Sun, H. T. Lv, Z. M. Wu, P. Wang, L. Liu and H. X. Cao, *J Pharmaceut Biomed*, 2008, **46**, 477-490.
19. X. J. Wang, H. Sun, A. H. Zhang, G. Z. Jiao, W. J. Sun and Y. Yuan, *Analyst*, 2011, **136**, 5068-5076.
20. X. J. Wang, A. H. Zhang, P. Wang, H. Sun, G. L. Wu, W. J. Sun, H. T. Lv, G. Z. Jiao, H. Y. Xu, Y. Yuan, L. Liu, D. X. Zou, Z. M. Wu, Y. Han, G. L. Yan, W. Dong, F. F. Wu, T. W. Dong, Y. Yu, S. X. Zhang, X. H. Wu, X. Tong and X. C. Meng, *Mol Cell Proteomics*, 2013, **12**, 1226-1238.
21. A. Dalcanton, A. Corradi, R. Stanziale, G. Maruccio and L. Migone, *Kidney Int*, 1979, **15**, 457-462.
22. X. Shengbin, W. Weiming and C. Nan, *Journal of Shanghai Jiaotong University (Medical Science)*, 2010, **30**, 752-757.

23. A. Martin, M. E. Ochagavia, L. C. Rabasa, J. Miranda, J. Fernandez-de-Cossio and R. Bringas, *Bmc Bioinformatics*, 2010, **11**.
24. H. Yongzheng, *Comprehensive natural products in traditional Chinese medicine*, Shanghai scientific & Technical Publishers, Shanghai, 2011.
25. C. A. Lipinski, F. Lombardo, B. W. Dominy and P. J. Feeney, *Adv Drug Deliver Rev*, 1997, **23**, 3-25.
26. D. S. Wishart, C. Knox, A. C. Guo, D. Cheng, S. Shrivastava, D. Tzur, B. Gautam and M. Hassanali, *Nucleic Acids Res*, 2008, **36**, D901-906.
27. H. Berman, K. Henrick, H. Nakamura and J. L. Markley, *Nucleic Acids Res*, 2007, **35**, D301-303.
28. A. Hamosh, A. F. Scott, J. S. Amberger, C. A. Bocchini and V. A. McKusick, *Nucleic Acids Res*, 2005, **33**, D514-D517.
29. K. G. Becker, K. C. Barnes, T. J. Bright and S. A. Wang, *Nat Genet*, 2004, **36**, 431-432.
30. M. Li, X. H. Sun, Z. H. Zhou, Z. Yu, S. G. Jin, X. J. Zhu and Y. Q. Gao, *J Ethnopharmacol*, 2013, **146**, 614-622.
31. C. Knox, V. Law, T. Jewison, P. Liu, S. Ly, A. Frolkis, A. Pon, K. Banco, C. Mak, V. Neveu, Y. Djoumbou, R. Eisner, A. C. Guo and D. S. Wishart, *Nucleic Acids Res*, 2011, **39**, D1035-D1041.
32. O. Trott and A. J. Olson, *J Comput Chem*, 2010, **31**, 455-461.
33. H. Y. Zhang, J. M. Jia, J. G. Cheng, F. Q. Ye, X. K. Li and H. C. Gao, *Mol Biosyst*, 2012, **8**, 595-601.
34. M. M. A. Alam, K. Javed and M. A. Jafri, *J Ethnopharmacol*, 2005, **96**, 121-125.
35. T. Yokozawa, K. Fujioka, H. Oura, G. Nonaka and I. Nishioka, *Nephron*, 1991, **58**, 155-160.
36. S. Lee, K. Park and D. Kim, *Expert Opin Drug Dis*, 2009, **4**, 1177-1189.
37. M. A. Yildirim, K. I. Goh, M. E. Cusick, A. L. Barabasi and M. Vidal, *Nature Biotechnology*, 2007, **25**, 1119-1126.
38. M. Zhu, L. Gao, X. Li, Z. C. Liu, C. Xu, Y. Q. Yan, E. Walker, W. Jiang, B. Su, X. J. Chen and H. Lin, *J Drug Target*, 2009, **17**, 524-532.
39. Y. Wang, X. Huang, Q. H. Liang, R. Fan, F. Qin, Y. Guo, K. P. Yan, W. Liu, J. K. Luo, Y. H. Li, X. L. Mao, Z. Q. Liu and H. H. Zhou, *Chin J Integr Med*, 2012, **18**, 690-698.
40. C. VanMen, Y. S. Jang, H. M. Zhu, J. H. Lee, T. N. Trung, T. M. Ngoc, Y. H. Kim and J. S. Kang, *Phytochem Analysis*, 2012, **23**, 359-364.
41. R. Song, Y. Cheng, Y. Tian and Z. J. Zhang, *Chin J Nat Medicines*, 2012, **10**, 275-278.
42. Y. N. A. Ni, R. M. Song and S. Kokot, *Anal Methods-Uk*, 2012, **4**, 171-176.
43. Y. Wang, X. Huang, Q. H. Liang, R. Fan, F. Qin, J. K. Luo, Y. H. Li, W. Liu, X. L. Mao, H. Ji, Z. Q. Liu, H. H. Zhou, L. Fan and L. C. Gao, *J Med Plants Res*, 2011, **5**, 2879-2885.
44. J. B. Wang, Y. Qin, W. J. Kong, Z. W. Wang, L. N. Zeng, F. Fang, C. Jin, Y. L. Zhao and X. H. Xiao, *Food Chem*, 2011, **129**, 1737-1743.

45. C. C. Lin, C. I. Wu, T. C. Lin and S. J. Sheu, *J Sep Sci*, 2006, **29**, 2584-2593.
46. M. Kuhn, D. Szklarczyk, S. Pletscher-Frankild, T. H. Blicher, C. von Mering, L. J. Jensen and P. Bork, *Nucleic Acids Res*, 2014, **42**, D401-D407.
47. H. Ye, L. Ye, H. Kang, D. F. Zhang, L. Tao, K. L. Tang, X. P. Liu, R. X. Zhu, Q. Liu, Y. Z. Chen, Y. X. Li and Z. W. Cao, *Nucleic Acids Res*, 2011, **39**, D1055-D1059.
48. R. C. Xue, Z. Fang, M. X. Zhang, Z. H. Yi, C. P. Wen and T. L. Shi, *Nucleic Acids Res*, 2013, **41**, D1089-D1095.
49. J. L. Ru, P. Li, J. N. Wang, W. Zhou, B. H. Li, C. Huang, P. D. Li, Z. H. Guo, W. Y. Tao, Y. F. Yang, X. Xu, Y. Li, Y. H. Wang and L. Yang, *J Cheminformatics*, 2014, **6**.
50. M. Tomita and K. Kami, *Science*, 2012, **336**, 990-991.
51. J. K. Nicholson and J. C. Lindon, *Nature*, 2008, **455**, 1054-1056.
52. P. M. Pryciak, *Science*, 2008, **319**, 1489-1490.
53. H. Kitano, *Science*, 2002, **295**, 1662-1664.
54. J. Boyle, *Nature*, 2013, **499**, 7-7.
55. C. Huang, Q. Ba, Q. Yue, J. Li, J. Li, R. Chu and H. Wang, *Mol Biosyst*, 2013, **9**, 3091-3100.
56. Y. H. Liu, *Kidney Int*, 2006, **69**, 213-217.
57. J. Yang, Z. Zeng, T. Wu, Z. C. Yang, B. Liu and T. Lan, *Exp Cell Res*, 2013, **319**, 3182-3189.
58. X. J. Li, W. H. Liu, Q. Wang, P. Q. Liu, Y. H. Deng, T. Lan, X. Y. Zhang, B. M. Qiu, H. R. Ning and H. Q. Huang, *Mol Cell Endocrinol*, 2009, **307**, 157-162.
59. R. Wang, Q. Wan, Y. Zhang, F. F. Huang, K. Z. Yu, D. M. Xu, Q. Wang and J. Sun, *Life Sci*, 2007, **80**, 2481-2488.
60. B. Zhu, Y. Lin, C. F. Zhu, X. L. Zhu, C. Z. Huang, Y. Lu, X. X. Cheng and Y. J. Wang, *Mol Med Rep*, 2011, **4**, 505-509.
61. D. Ray, E. C. Osmundson and H. Kiyokawa, *The Journal of biological chemistry*, 2006, **281**, 23060-23065.
62. S. A. Wagner, P. Beli, B. T. Weinert, M. L. Nielsen, J. Cox, M. Mann and C. Choudhary, *Mol Cell Proteomics*, 2011, **10**.
63. S. Rahman, Y. Patel, J. Murray, K. V. Patel, R. Sumathipala, M. Sobel and E. S. Wijelath, *Bmc Cell Biol*, 2005, **6**.
64. F. Ernst, S. Hetzel, S. Stracke, D. Czock, G. Vargas, M. P. Lutz, F. Keller and P. M. Jehle, *Eur J Clin Invest*, 2001, **31**, 1029-1039.
65. J. McLarty, R. L. H. Bigelow, M. Smith, D. Elmajian, M. Ankem and J. A. Cardelli, *Cancer Prev Res*, 2009, **2**, 673-682.
66. J. Su, L. P. Yin, X. Zhang, B. B. Li, L. Liu and H. Li, *Transpl P*, 2013, **45**, 2546-2552.
67. L. D. Kong, C. H. K. Cheng and R. X. Tan, *J Ethnopharmacol*, 2004, **91**, 351-355.
68. J. S. Hwang, S. A. Lee, S. S. Hong, K. S. Lee, M. K. Lee, B. Y. Hwang and J. S. Ro, *Arch Pharm Res*, 2005, **28**, 190-194.

69. A. A. Eddy, *Adv Chronic Kidney D*, 2005, **12**, 353-365.
70. T. Iwaki, T. Urano and K. Umemura, *Brit J Haematol*, 2012, **157**, 291-298.
71. Y. L. Cao, D. F. Wang, X. L. Wang, J. Zhang, Z. Y. Shan and W. P. Teng, *J Cardiovasc Pharm*, 2013, **62**, 452-456.
72. L. H. Abou-Agag, M. L. Aikens, E. M. Tabengwa, R. L. Benza, S. R. Shows, H. E. Grenett and F. M. Booyse, *Alcohol Clin Exp Res*, 2001, **25**, 155-162.
73. C. M. Turner, N. Arulkumaran, M. Singer, R. J. Unwin and F. W. K. Tam, *Bmc Nephrol*, 2014, **15**.
74. J. M. Poth, K. Brodsky, H. Ehrentraut, A. Grenz and H. K. Eltzschig, *J Mol Med*, 2013, **91**, 183-193.
75. D. Sen, A. Chapla, N. Walter, V. Daniel, A. Srivastava and G. R. Jayandharan, *J Thromb Haemost*, 2013, **11**, 293-306.
76. W. W. Lan, A. Petznick, S. Heryati, M. Rifada and L. Tong, *Ocular Surface*, 2012, **10**, 137-148.
77. M. L. Lin, J. G. Chung, Y. C. Lu, C. Y. Yang and S. S. Chen, *Oral Oncol*, 2009, **45**, 531-537.
78. G. Q. Meng, Y. Y. Liu, C. C. Lou and H. Yang, *Brit J Pharmacol*, 2010, **161**, 1628-1644.
79. Y. Zhang, S. Fan, N. Hu, M. Gu, C. Chu, Y. Li, X. Lu and C. Huang, *PPAR research*, 2012, **2012**, 374936.
80. D. W. Shin, S. N. Kim, S. M. Lee, W. Lee, M. J. Song, S. M. Park, T. R. Lee, J. H. Baik, H. K. Kim, J. H. Hong and M. Noh, *Biochem Pharmacol*, 2009, **77**, 125-133.
81. C. E. Hills and P. E. Squires, *Cytokine Growth F R*, 2011, **22**, 131-139.
82. E. Vasyutina and M. Treier, *Semin Cell Dev Biol*, 2010, **21**, 831-837.
83. J. M. R. Danielsen, K. B. Sylvestersen, S. Bekker-Jensen, D. Szklarczyk, J. W. Poulsen, H. Horn, L. J. Jensen, N. Mailand and M. L. Nielsen, *Mol Cell Proteomics*, 2011, **10**.
84. P. Sridevi, H. Alexander, E. L. Laviad, Y. Pewzner-Jung, M. Hannink, A. H. Futerman and S. Alexander, *Bba-Mol Cell Res*, 2009, **1793**, 1218-1227.
85. L. K. Povlsen, P. Beli, S. A. Wagner, S. L. Poulsen, K. B. Sylvestersen, J. W. Poulsen, M. L. Nielsen, S. Bekker-Jensen, N. Mailand and C. Choudhary, *Nat Cell Biol*, 2012, **14**, 1089-+.
86. G. Q. Xu, J. S. Paige and S. R. Jaffrey, *Nat Biotechnol*, 2010, **28**, 868-U154.
87. J. D. Humphries, A. Byron, M. D. Bass, S. E. Craig, J. W. Pinney, D. Knight and M. J. Humphries, *Sci Signal*, 2009, **2**.
88. W. Kim, E. J. Bennett, E. L. Huttlin, A. Guo, J. Li, A. Possemato, M. E. Sowa, R. Rad, J. Rush, M. J. Comb, J. W. Harper and S. P. Gygi, *Mol Cell*, 2011, **44**, 325-340.
89. N. D. Udeshi, D. R. Mani, T. Eisenhaure, P. Mertins, J. D. Jaffe, K. R. Clauser, N. Hacohen and S. A. Carr, *Mol Cell Proteomics*, 2012, **11**, 148-159.
90. A. M. Yu, C. P. Granvil, R. L. Haining, K. W. Krausz, J. Corchero, A. Kupfer, J. R. Idle and F. J. Gonzalez, *J Pharmacol Exp Ther*, 2003, **304**, 539-546.

91. A. P. Il'chenko, N. V. Shishkanova, O. G. Chernyavskaya and T. V. Finogenova, *Microbiology+*, 1998, **67**, 241-244.
92. C. G. Mao, R. J. Xu, A. Bielawska and L. M. Obeid, *J Biol Chem*, 2000, **275**, 6876-6884.
93. J. Koch, S. Gartner, C. M. Li, L. E. Quintern, K. Bernardo, O. Levran, D. Schnabel, R. J. Desnick, E. H. Schuchman and K. Sandhoff, *J Biol Chem*, 1996, **271**, 33110-33115.
94. J. Wang, K. K. Huo, L. X. Ma, L. J. Tang, D. Li, X. B. Huang, Y. Z. Yuan, C. H. Li, W. Wang, W. Guan, H. Chen, C. Z. Jin, J. C. Wei, W. Q. Zhang, Y. S. Yang, Q. M. Liu, Y. Zhou, C. L. Zhang, Z. H. Wu, W. X. Xu, Y. Zhang, T. Liu, D. H. Yu, Y. P. Zhang, L. Chen, D. W. Zhu, X. Zhong, L. X. Kang, X. Gan, X. L. Yu, Q. Ma, J. Yan, L. Zhou, Z. Y. Liu, Y. P. Zhu, T. Zhou, F. C. He and X. M. Yang, *Mol Syst Biol*, 2011, **7**.
95. T. J. Sun, K. Hayakawa, K. S. Bateman and M. E. Fraser, *Journal of Biological Chemistry*, 2010, **285**, 27418-27428.
96. Q. W. Group, *Quantitative and Systems Pharmacology in the Post-genomic Era: New Approaches to Discovering Drugs and Understanding Therapeutic Mechanisms*, NIH, 2011.
97. J. K. Nicholson, J. C. Lindon and E. Holmes, *Xenobiotica; the fate of foreign compounds in biological systems*, 1999, **29**, 1181-1189.